

The Extinction Towards the GRB970228 Field

Francisco J. Castander and Donald Q. Lamb

Department of Astronomy and Astrophysics, University of Chicago,
5640 S Ellis Ave, Chicago, IL 60637

ABSTRACT

We determine the local galactic extinction towards the field of gamma-ray burst GRB970228 using a variety of methods. We develop a maximum likelihood method for measuring the extinction by comparing galaxy counts in the field of interest to those in a field of known extinction, and apply this method to the GRB970228 field. We also measure the extinction by comparing the observed stellar spectral energy distributions of stars in the GRB970228 field to the spectral energy distribution of library spectra of the same spectral type. Finally we estimate the extinction using the Balmer emission line ratios of a galaxy in the GRB970228 field, and the neutral hydrogen column density and amount of infrared dust emission toward this field. Combining the results of these methods, we find a best-fit galactic extinction in the optical of $A_V = 1.19^{+0.10}_{-0.17}$, which implies a substantial dimming and change of the spectral slope of the intrinsic GRB970228 afterglow.

Subject headings: gamma rays: bursts — extinction

1. Introduction

GRB970228 is the first gamma-ray burst (GRB) for which a counterpart at longer wavelengths has been detected, and extensive follow-up observations of it have been made. GRB970228 was detected by the BeppoSAX satellite on 1997 February 28 (Costa et al. 1997a). Subsequent BeppoSAX follow-up observations revealed a rapidly fading X-ray source (Costa et al. 1997b). Later, ASCA (Yoshida et al. 1997) and ROSAT (Frontera et al. 1997, 1998) observations showed that it continued to fade in X-rays over a two week period.

Ten days after the burst, Groot et al. (1997a) announced the detection of a fading source which was the first optical counterpart of a GRB. Frenetic activity followed, with new observations being taken and previous ones being reanalyzed, which led to reports of several detections in the optical and near infrared (Groot et al. 1997b; Metzger et al. 1997a; van Paradijs et al. 1997; Metzger et al. 1997b; Klose et al. 1997; Margon et al. 1997; Soifer et al. 1997; Metzger et al. 1997b; Pedichini et al. 1997; Djorgovski et al. 1997). Observations with the Hubble Space Telescope made another startling discovery. The fading GRB afterglow was spatially coincident with an extended source (Sahu et al. 1997a; Sahu et al. 1997b; Fruchter et al. 1997).

Wijers et al. (1997) and Reichart (1997) discussed early observations of GRB970228 in the context of theoretical models. They found that the behavior of the GRB afterglow was consistent with the expectations of relativistic fireball models. In one of the simplest models, the afterglow power-law temporal decay is simply related to its power-law spectrum by a factor of 1.5, which was consistent with the early measurements that were being reported. Later, Galama et al. (1997, 1998) compiled the most relevant photometric measurements of GRB970228, converting them into a single photometric band when necessary and subtracting the contribution of the extended source component. They fit the optical transient temporal evolution to a power-law with $\alpha = -1.10 \pm 0.04$ ($\chi_r^2 = 2.3$ for 9 degrees of freedom).

For the first time, temporal, as well as spatial, coincidence could be used to associate X-ray and optical sources with GRBs. Since then several other GRB afterglows have been detected and monitored, and it now seems firmly established that these fading X-ray and optical sources are counterparts of the bursts. In this paper, we determine the galactic extinction towards GRB970228, performing a careful analysis of the publicly available observations. The goal we have in mind is to better understand the intrinsic properties of this afterglow. In a companion paper (Castander & Lamb 1998), we discuss the implications of our measurements for the properties and nature of the point-like and extended optical sources coincident with the fading X-ray source.

This paper is organized as follows. First, we utilize various methods to measure the extinction at optical wavelengths. In §2 we describe a photometric method: we compute the galaxy number counts in the GRB970228 HST WFPC2 observations and compare them to the number counts in the Hubble Deep Field (HDF; Williams et al. 1996). In the next section we describe spectroscopic methods that use the Keck II observations made by Tonry et al. (1997). In §3.1 we measure the Balmer series emission lines of a galaxy 64" away from the GRB and estimate the extinction from the observed relative intensities of these emission lines. In §3.2 we use three stars that lie 2.9", 16.8" and 42.7" away from the GRB. We determine their spectral types and compute the extinction value required to make their measured spectral energy distributions consistent with their spectral types. Secondly, we estimate the extinction from measurements of the column density of hydrogen gas and dust emission measurements, using established correlations. In §4 we utilize hydrogen column density measures and in §5 the infrared 100 μm dust emission. We discuss our results in §6 and present our conclusions in §7.

2. Galaxy number counts

Galaxy number counts can be used to measure directly the relative extinction between two fields. The idea is simple. The observed apparent optical magnitude of a galaxy is increased (the flux is decreased) because its radiation is absorbed by material, normally dust for optical extinction, along the line of sight. Because the number of observed galaxies increases with magnitude, number counts are reduced if extinction is present. Ignoring possible deviations due to galaxy clustering and sampling effects, in a given magnitude range and in a given filter, the number of galaxies should

be the same irrespective of direction. Galaxy number counts are normally approximated as

$$N(m_1 < m < m_2) = C10^{\alpha m}, \quad (1)$$

where the values of the normalization, C , and the slope, α , depend on the specific filter and magnitude range. However, due to extinction, the observed apparent magnitude will be increased to $m_{obs} = m + A$. Therefore, if we compare two different fields with extinctions A_1 and A_2 , their relative number counts in the same observed apparent magnitude range will be

$$\frac{N_1(m_1 < m_{obs} < m_2)}{N_2(m_1 < m_{obs} < m_2)} = \frac{C_1}{C_2} 10^{\alpha_1(m+A_1) - \alpha_2(m+A_2)}. \quad (2)$$

One can assume that the normalizations and slopes are the same, if the galaxy number counts are measured in the same unextinguished apparent magnitude range and in the same filter. If we additionally assume that surface brightness dimming effects do not alter the relative number counts, then the ratio of the number counts depends only on the relative extinction and common slope

$$\frac{N_1(m_1 + A_1 < m_{obs} < m_2 + A_1)}{N_2(m_1 + A_2 < m_{obs} < m_2 + A_2)} = 10^{\alpha(A_2 - A_1)}. \quad (3)$$

In the present case we wish to estimate the extinction towards GRB970228 by comparing the number counts of the GRB WFPC2 HST observations with those of another field of known extinction. We have chosen the Hubble Deep Field (Williams et al. 1996) because it is the best studied and deepest field for which the extinction is already known, having been observed with the same instrument.

GRB970228 was observed by HST on 1997 March 26th and April 7th. In both observations the optical counterpart was centered in the middle of the PC1 CCD, but there was a 2.40 deg difference in rotation angle between the first and second observations. At both epochs, four exposures were taken in the F606W filter and two exposures in the F814W filter, totalling 4700 and 2400 seconds, respectively (Sahu et al. 1997c). The HDF was observed for 109050 and 123600 seconds in the F606W and F814W filters respectively (for more details see Williams et al. 1996).

Our starting point was the HST archive, from which we retrieved the observations of both fields. After the standard pipeline reduction, we combined the different exposures at each epoch of the GRB970228 field using the IRAF/STSDAS task CRREJ. Then the combined second epoch image was rotated according to the difference in the ORIENTAT header keyword and shifted using sub-pixel shifts and fourth-order polynomial interpolation, according to the measured centroid positions of stars. Subsequently, both epochs were combined using the IRAF task IMCOMBINE, rejecting pixels that were deviant from the median by more than 5 sigma, the noise being characterized by the square root of the median plus the square of the read-out noise. However, for this last step to be

effective the sky values had to be rescaled because the direction of the April 7th observations was closer to the Sun than was the direction of the previous ones, and the images had background count values approximately 25% higher. This last rejection process affected only $\sim 0.12\%$ and $\sim 0.35\%$ of the pixels in the F606W and F814W images, respectively. The HDF images retrieved had already been processed and no further reduction was done.

In order to reduce the systematic errors in selecting galaxies and measuring their magnitudes, we chose to analyze both fields using the same procedures. We used the SExtractor image analysis package (Bertin & Arnouts 1996) to automatically detect and measure object magnitudes. The magnitude zero points were computed using the PHOTFLAM and PHOTZPT image header keywords, taking into account the different effective gains of the four WFPC2 CCDs (Holtzman et al. 1995). These ST magnitudes were converted to AB magnitudes¹ using the transformations: $(V_{606})_{AB} = (V_{606})_{ST} - 0.199$ and $(I_{814})_{AB} = (I_{814})_{ST} - 0.819$. After generating catalogs of extracted objects and their magnitudes, all objects brighter than $V_{606} = 26.5$ and $I_{814} = 25.9$ were visually inspected and spurious objects were removed. This process was crucial in the F814W image of the GRB970228 field because combining only four exposures precluded an accurate rejection of “hot pixels”. The different rotation angles between the March 26 and April 7 images of the GRB970228 field and the small dithering in the HDF made it necessary to exclude the edges of the CCD fields as well. After generating the catalogs, we compared our galaxy number counts in the HDF field with those obtained by the HDF team, in order to check our object selection criteria and our magnitude measurements. The galaxy number counts in both filter images were consistent with each other.

In order to estimate the relative extinction between the two fields, we utilize a maximum likelihood method. We construct a joint likelihood function that is the product of four likelihoods, each one being the likelihood that a given galaxy catalogue with its measured magnitudes and errors resembles a power-law distribution (see equation 1) in a given magnitude range. The four likelihood functions correspond to V_{606} and I_{814} images of the two fields. Therefore our joint likelihood function has 8 parameters: the normalizations and slopes in each of the four combinations of images and filters $(C_{606}^{HDF}, \alpha_{606}^{HDF}, C_{606}^{GRB}, \alpha_{606}^{GRB}, C_{814}^{HDF}, \alpha_{814}^{HDF}, C_{814}^{GRB}, \alpha_{814}^{GRB})$. However, if we analyze the catalogues in the same unextinguished apparent magnitude range (which requires us to know the extinction a priori; see equation 3), we can assume that the slopes are the same in the HDF and GRB970228 fields in a given filter image, and that the normalizations are therefore related by

$$\begin{aligned}
\alpha_{606}^{GRB} &= \alpha_{606}^{HDF}, \\
\alpha_{814}^{GRB} &= \alpha_{814}^{HDF}, \\
C_{606}^{GRB} &= C_{606}^{HDF} 10^{\alpha(A_{606}^{HDF} - A_{606}^{GRB})}, \\
C_{814}^{GRB} &= C_{814}^{HDF} 10^{\alpha(A_{814}^{HDF} - A_{814}^{GRB})}.
\end{aligned} \tag{4}$$

¹All magnitudes quoted in this paper are in the AB magnitude system

If we further assume that the extinction behaves like extinction law typical of the interstellar medium (Cardelli et al. 1987, O’Donnell 1994), we can impose a further constraint by integrating the extinction law with the filter responses

$$\begin{aligned} A_{606} &= 0.919 A_V, \\ A_{814} &= 0.608 A_V. \end{aligned} \tag{5}$$

Then the joint likelihood function has only 5 parameters: two slopes, two normalizations, and the difference in the extinction. We can marginalize this likelihood function over both normalizations (F606W and F814W) and use the measured value of the extinction in the HDF field, $A_V = 0.0$ (Williams et al. 1996), in order to reduce the maximization required to three parameters (α_{606} , α_{814} , A_V).

As mentioned before, we need to know *a priori* the value of the extinction in order to choose the magnitude ranges for which our parameter reduction is valid. Therefore, we proceed in the following iterative way. We start by choosing a value for the extinction (a good initial guess can be made by comparing the counts in different magnitudes ranges). We then correct the observed magnitudes for that extinction value and plot the resulting cumulative number counts distributions. Since the HDF field has longer exposures and goes much deeper, we can compute the extinction-corrected magnitude at which the GRB970228 field counts start to be incomplete, compared to the HDF field. Plotting the cumulative number counts of both extinction-corrected datasets gives a good indication where the incompleteness starts to affect the GRB970228 field. We adopt as our faint limiting magnitude the magnitude at which the cumulative counts deviate by more than 10% in the F606W filter and 15% in the F814W filter (the errors in the computed magnitudes are larger in the F814W filter and that is why the deviation allowed is larger as well). Note that the deviation in the F814W filter depends on the bright magnitude limit adopted as the HSD and GRB counts differ at the lower I_{814} magnitudes measured (see Figure 1). We also check the probability as a function of limiting magnitude that both cumulative magnitude distributions are drawn from the same parent distributions, using the KS test. At our adopted cut and taking into account our bright magnitude limit as well, the hypothesis that the two count distributions come from the same parent distribution cannot be rejected at even the 1σ confidence level. Once we have determined the limiting extinction-corrected magnitude, we use it, without the extinction correction, as the faintest magnitude down to which we compute the joint likelihood function. We take as the bright magnitude limit the magnitude at which the number counts fall below $\sim 7.5 \times 10^4 \text{ mag}^{-1} \text{ deg}^{-2}$ (~ 10 objects per magnitude in the whole WFPC2 area). We then maximize the likelihood function and obtain the best-fit values for the slopes and the extinction. Starting with this new value for the extinction, we iterate until the process converges.

It is worth noting that our final value for the extinction is almost independent of the bright magnitude limit adopted. The exact faint magnitude limit adopted does not affect the final value

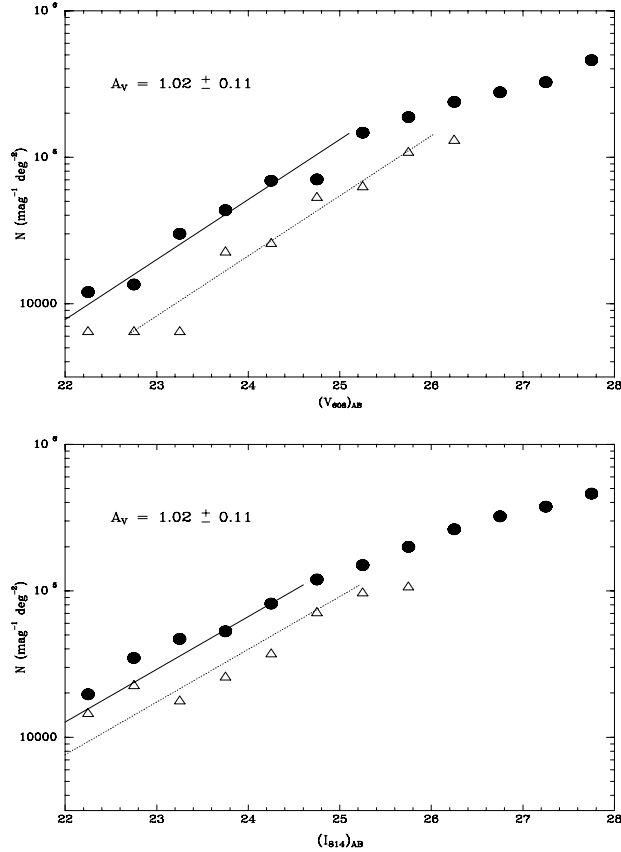


Fig. 1.— Number counts in the HDF (filled circles) and GRB970228 (open triangles) fields. The top and bottom figures correspond to the V_{606} and I_{814} filters respectively. Error bars are omitted for clarity. The solid and dotted lines represent the best fit slope values in the combined maximum likelihood method. They are plotted only in the regions where the fit was performed. Note that they are not independent (see text for details).

of extinction either, because we perform a correction for possible incompleteness *a posteriori* (see below).

Figure 1 illustrates our results. After a few iterations, we obtain values for the extinction and number counts slopes of $A_V = 1.02 \pm 0.11$, $\alpha_{606} = 0.41 \pm 0.1$, and $\alpha_{814} = 0.36 \pm 0.1$. The magnitude ranges used are $21.8 < V_{606}^{HDF} < 25.1$, $22.72 < V_{606}^{GRB} < 26.02$, $21.0 < I_{814}^{HDF} < 24.6$, and $21.61 < I_{814}^{GRB} < 25.21$.

So far we have neglected any possible effects introduced by the dimming of the surface brightnesses of galaxies due to the optical extinction. In the present case, the GRB field is considerably obscured compared to the HDF and therefore low surface brightness objects could be missed in the GRB field because they fall below the detection limit when they should have been included in

Figure available at:

<http://astro.uchicago.edu/home/web/fjc/figures/CL98a/CL98a.fig2.eps>

Fig. 2.— Slit position of the Keck II spectroscopic observations of the GRB970228 field (Tonry et al. 1997). The distance from S2 to S3 is $59.5''$.

the magnitude limits considered. This effect would lead to an overestimation of the extinction. In order to correct for it, we simulate WFPC2 fields by degrading the WFPC2 HDF images according to several values of the extinction and then carry out the same analysis on these simulated images as we have on the GRB field images. According to our simulations, we overestimate the value of the extinction by approximately 15%.

Our extinction estimate could also be affected by clustering if one of the fields we have chosen to study is more or less strongly clustered compared to the other. The integral of the two point angular correlation function gives an estimate of the extra variance introduced by clustering in the number counts. In the magnitude range studied here, the two point angular correlation function can be approximated by $\omega(\theta'') \sim 1.0 \theta''^{-0.8}$ (Brainerd & Smail 1998). Integrating over the WFC2 area studied, we find that the angular clustering on the sky adds a small contribution to the variance in the counts at the magnitude range studied. If we include this additional variance contribution into our maximum likelihood method and also take into account the previous $\sim 15\%$ correction factor, we obtain a revised extinction value of $A_V = 0.89 \pm 0.13$, where the estimated error includes the contribution of our correction factor as well as the contribution resulting from our *clustering-modified* maximum likelihood method.

3. Spectroscopic methods

Spectroscopy of the GRB optical afterglow was attempted using the Keck II telescope by Tonry et al. (1997). Although they could not obtain a spectrum with sufficient signal-to-noise to discern the nature of the optical counterpart, they obtained spectra of several other nearby objects that fell within the long slit they used (see Figure 2).

We retrieved the spectroscopic data from the Hawaii public FTP directory and reduced them. Observations had been taken with the Low Resolution Imaging Spectrograph (LRIS) in six exposures on March 31.25 UT (500 s and 1000 s), April 1.25 UT (1000 s and 1000 s) and April 2.25 UT (1000 s and 1000 s). The instrument configuration used was the 300 lines/mm grating, blazing at 5000 \AA , giving a dispersion of $\sim 2.5 \text{ \AA/pixel}$ and an approximate wavelength coverage $4300\text{-}9500 \text{ \AA}$. The slit was $1.0''$ wide and $2.9'$ long. It was centered at the star $2.9''$ East of the optical counterpart (S1) and moved $10''$ Eastward in two of the exposures. The position angle was 86.4 degrees.

The spectroscopic images were processed using standard IRAF routines. We combined the observations into one image, shifting the offset images and rejecting cosmic rays. The resulting

optimally-extracted spectra were found to be insensitive to the type of shift applied: fractional or integer pixel shifts. Six objects fell, totally or partially, within the slit and produced dispersed spectra in the 2-dimensional images. Figure 2 shows where the slit was placed in the sky and the objects for which spectra were obtained. We did not include in the final combined image the observations taken on March 31.25 UT, due to their poorer quality. The total exposure used was then 4000 s.

We extracted the spectra with our own implementation of Horne’s optimal extraction algorithm (Horne 1986). Spectra were wavelength-calibrated with He-Ne arcs and flux calibrated with the spectrophotometric standard Hiltner 600. We obtained spectrophotometric colors convolving the flux calibrated spectra with the WFPC2 filter responses. Comparing these to the photometric colors measured in the WFPC2 HST image we found our relative flux calibration errors to be lower than 5% (see Table 1).

3.1. Balmer series emission line ratios of galaxies

The flux ratios of the Balmer emission lines of galaxies can be used to characterize the optical extinction. The H_α/H_β and H_γ/H_β ratios of emission-line galaxies depend on the conditions within that galaxy. Theoretically, for typical galaxy conditions, these values are 2.88 and 0.46 respectively (Osterbrook 1989). The measured values, however, will differ due to the intrinsic extinction within the galaxy at redshift z and to the local extinction in our own galaxy. Once the Balmer line flux ratios are measured, and assuming a typical extinction law, one can compute both the intrinsic and the local extinction values.

In the Keck II spectroscopic observations, the two galaxies that happened to lie within the slit exhibited emission lines. However, only the spectrum of the galaxy G2, at redshift $z = 0.3792$, had a large enough signal-to-noise ratio to allow reliable measurements of the Balmer emission line fluxes (Figure 3). We measure the following Balmer line flux ratios: $H_\alpha/H_\beta = 5.60_{-0.32}^{+0.36}$ and $H_\beta/H_\gamma = 0.35_{-0.18}^{+0.12}$, where the errors are mainly due to the uncertainty in estimating the continuum. Assuming a standard value for these ratios of 2.88 and 0.465 (Osterbrook 1989) and a typical extinction law for diffuse interstellar medium, $R_V = 3.1$ (Cardelli et al. 1987), we can obtain the values for the extinction intrinsic to the galaxy and within our own galaxy. Figure 4 shows the values allowed with our measured ratios and assumptions. Our best values are: $A_V(z = 0.3792) = 0.901$ and $A_V(z = 0.0) = 1.276$. However, due to the uncertainties in the ratios and the almost parallel constraints that the ratios place in the $A_V(z = 0.3792)$ vs. $A_V(z = 0.0)$ plane, a wide range of values are allowed (Figure 4).

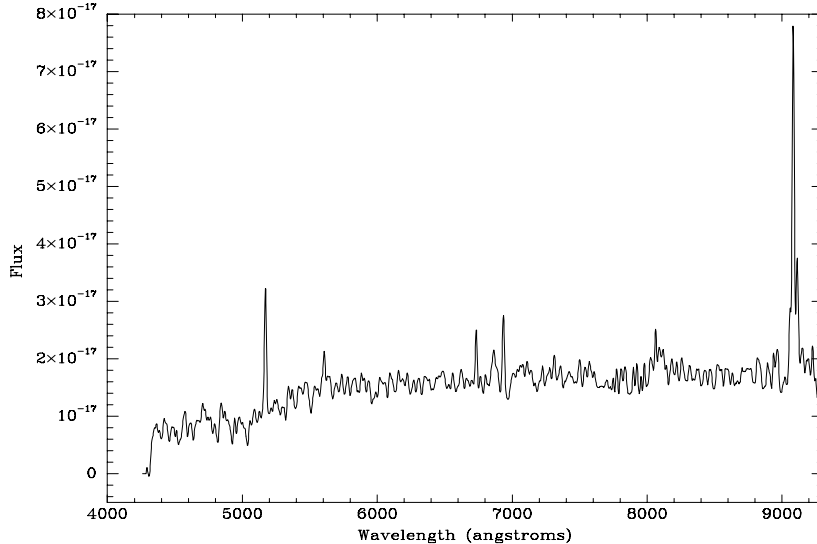


Fig. 3.— Slightly smoothed spectrum of galaxy G2 at redshift $z = 0.3792$.

3.2. Stellar spectral energy distributions versus spectral types

Another method that can be used to estimate the extinction in this field is to compare the spectral energy distributions and spectral types of stars observed spectroscopically. If the spectral type can be reliably determined without color or spectral continuum information, then one can infer the extinction by finding the best fit of the extinction-corrected spectrum (either in color or continuum spectral distribution) to library spectra of the same spectral type, with the extinction correction as a fitting parameter.

As mentioned before, three stars were observed spectroscopically (two accidentally) with the Keck II telescope by Tonry et al. (1997) (Figure 2). The signal-to-noise ratios achieved in the 6000-7000 Å spectral region were 3.7, 11.5 and 1.3 for stars S1, S2 and S3, respectively.

These stars were also observed within the WFPC2 HST pointings of the GRB970228 field. Table 1 summarizes the magnitudes and colors measured for these stars. The apparent magnitudes indicate that these stars are most likely to be dwarfs. If they were giants, their apparent magnitudes would imply that their distances are larger than 100 kpc in order to be consistent with absolute magnitudes of giant stars of the same spectral type. Such distances are highly unlikely.

In order to classify these stars, we compare them with the stellar spectral atlases of Jacoby et al. (1984) and Silva & cornell (1992). Given the wavelength coverage and the low signal-to-noise ratio of the stellar spectra, there are only a few features that can be used to classify these stars. The wavelength coverage does not allow us to use features bluewards of H_{β} . We classify S1 in a spectral class between K3v and K5v, S2 between K4v and K7v and S3 between M0v and M3v. The K-star classifications are mainly based on the Mg $\lambda 5174$ and Na $\lambda 5893$ W_f indexes (Prichet & van

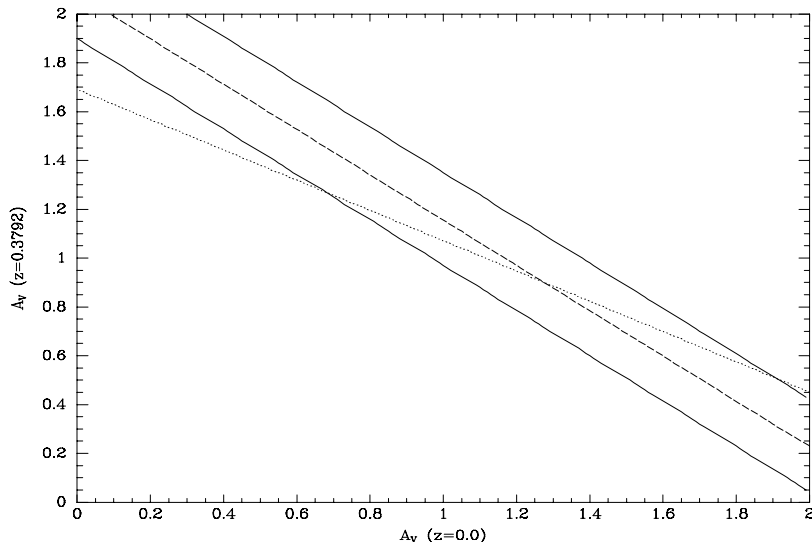


Fig. 4.— Balmer ratio constraints on the internal extinction within galaxy G2 at $z = 0.3792$ and the extinction due to our own galaxy. The constraint for a ratio is degenerate in this extinction-extinction plane. The dashed line gives the best fit extinction values based on the H_α/H_β ratio and the solid line its 1σ error. The dotted line, the H_β/H_γ ratio constraint. Due to the uncertainty of this ratio measurement no 1σ errors are plotted. The best values obtained are $A_V(z = 0.3792) = 0.901$ and $A_V(z = 0.0) = 1.276$. However these values are only constrained by the H_α/H_β ratio region.

den Bergh 1977), and on the presence or absence of TiO, VO and CaH bands (e.g., Kirkpatrick et al. 1991).

We have also attempted a more automatic classification, based only on line information. We fit and subtracted a continuum to the observed stars and to the template spectra. We then computed a metric distance (treating the spectra as vectors; e.g., Vieira & Ponz 1995) between the observed spectra and the templates. We also computed a standard χ^2 between the observed continuum-subtracted spectra and the continuum-subtracted library spectra. Both methods produce similar results. The spectral types that give the minimum metric distances and values of χ^2 for our stars are: S1, from K1v to K7v; S2, from K2v to K5v and S3, from M0v to M4v, although the constraints for S3 are rather weak.

Taking into consideration our visual classification, the measured spectral indexes and the automatic classification allowed types, we estimate the value of the extinction for each star by reddening the template spectra to fit the spectral distribution of our observed stars. In order to avoid possible problems with sky subtraction, we have used only the wavelength region from 4500 – 7500 Å in the fitting procedure. Figure 5 illustrates the comparison between the observed and reddened library spectra.

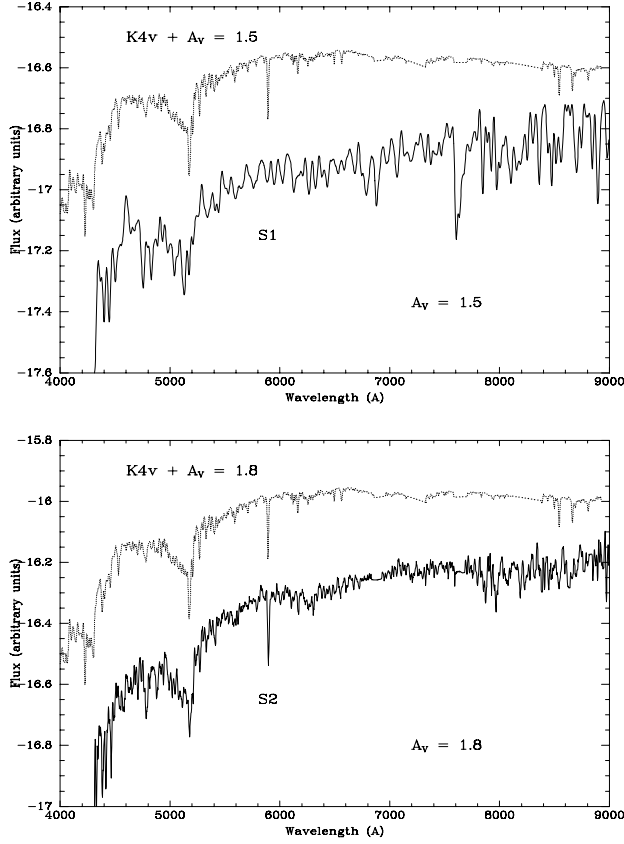


Fig. 5.— Spectra of stars S1 (top) and S2 (bottom). The solid lines correspond to the observed star spectra, while the dotted lines are the library spectra reddened to match the observed spectra (see text for details).

For S1, we obtained $A_V = 1.5^{+0.4}_{-0.9}$ with the best value corresponding to a K4v star and the allowed range corresponding to K1v and K7v stars. For S2, we get $A_V = 1.8^{+0.2}_{-0.5}$ with the best value corresponding to a K4v star, and the allowed range to a K2v star and an intermediate K5v-K7v star. For S3, $A_V = 1.8^{+0.5}_{-1.0}$, the best value corresponds to a M2v star and the allowed range to M0v and M3v stars. The errors quoted include in quadrature the uncertainty in the stellar spectral fit, given by the allowed ranges of spectral types, and an estimate of the uncertainty contributed by the spectrophotometric calibration.

Finally, we compute our best estimate of the extinction by combining the contributions of the three stars weighting them by their signal-to-noise. We obtain a value of $A_V = 1.73^{+0.20}_{-0.42}$.

4. Extinction from neutral hydrogen column density

BeppoSAX detected the GRB970228 afterglow in X-rays with both the MECS and LECS instruments (Costa et al. 1997b). In the first set of observations, eight hours after the burst, the measured flux was bright enough to fit a spectrum to the measured counts in the 0.1-10 keV energy band. The best fit was obtained for a power-law spectrum with photoelectric absorption of $N_H = 3.5_{-2.3}^{+3.3} \times 10^{21} \text{ cm}^{-2}$ (Frontera et al. 1998). Converting this value to color excess (see below), and assuming that all of the absorption is due to our own galaxy, would imply a color excess of $E(B - V) = 0.73_{-0.48}^{+0.69}$ and an optical extinction of $A_V = 2.26_{-1.48}^{+2.13}$.

Searching published HI surveys, we find values for the neutral hydrogen column density of 1.60×10^{21} and $1.59 \times 10^{21} \text{ cm}^{-2}$ from Stark et al. (1992) and Dickey & Lockman (1990), respectively. Adopting the conversion factor between HI and color excess of $4.8 \times 10^{21} \text{ cm}^{-2} \text{ mag}^{-1}$ (Bohlin et al. 1978), we obtain $E(B - V) = 0.33$. This conversion factor is almost the same as that obtained by Heiles (1976) and somewhat lower than that of Knapp & Kerr (1974). According to Bohlin et al. (1978), although they do not quote a formal error, their conversion factor should be accurate to within a factor of 1.5 for the total (HI+H₂) hydrogen column density. Comparing their total and neutral hydrogen plots against color excess, the neutral hydrogen column density shows a larger dispersion. Nevertheless, adopting a factor of 1.5 would give a color excess of $E(B - V) = 0.33 \pm 0.13$. If instead we adopt the calibration of Heiles (1976) for which the author gives errors, a value of neutral hydrogen column density of $1.60 \times 10^{21} \text{ cm}^{-2}$ would yield a color excess of $E(B - V) = 0.29 \pm 0.03$. The difference between these two values is due to a zero point difference in the relation.

However, other methods of determining the color excess give slightly different values. For example, Burstein & Heiles (1982), using a combined HI column density/galaxy number counts method, get a value of $E(B - V) = 0.23$, using the Heiles (1975) and Heiles & clearly (1979) HI measurements and the smoothed Shane & Wirtanen (1967) galaxy counts. If instead of using the hydrogen column density value used by Burstein & Heiles (1982), we use the Stark (1992) and Dickey & Lockman (1990) value, adopting the conversion factor employed by Burstein & Heiles (1982), and the value they give for the smoothed galaxy counts from Shane & Wirtanen (1967) we obtain $E(B - V) = 0.25 \pm 0.09$.

The error in the neutral hydrogen column density measurement is negligible compared to the error in its relation to reddening, and therefore should not add significant uncertainty to the color excess value derived. However, the resolution of the HI maps is poor, around 1 or 2 degrees. The Dickey & Lockman 1990 21 cm HI map of the GRB970228 field is shown in Figure 6. As can be seen, the GRB970228 is in a region showing a relatively steep HI gradient on angular scales of a few degrees and it is quite conceivable that there are significant deviations on small angular scales from the value assumed.

Taking into account these considerations, we conservatively adopt a value of $E(B - V) = 0.30 \pm 0.13$. Assuming an extinction law typical of the diffuse interstellar medium, $R_V \equiv A_V/E(B - V) =$

Figure available at:

<http://astro.uchicago.edu/home/web/fjc/figures/CL98a/CL98a.fig6.eps>

Fig. 6.— Hydrogen column density (left) and IRAS 100 micron (right) maps. Both are $8.5^\circ \times 8.5^\circ$. Their resolutions are $\sim 1^\circ$ and $\sim 5'$, respectively. The white circle (40' diameter) is centered on the position of the GRB970228 optical transient. The bright regions correspond to strong emission, the dark regions to weak emission. North is up and East to the left on both images. A strong emission gradient is noticeable in the GRB970228 region.

3.1 (Cardelli et al. 1987, O'Donnell 1994), this gives an extinction value of $A_V = 0.93 \pm 0.39$.

5. Extinction from infrared emission

The optical extinction is also known to correlate with infrared emission at long wavelengths ($\sim 100\mu m$). However, this correlation shows substantial scatter because the infrared emission is dependent on the radiation field and the temperature of the dust grains (e.g., Boulanger & Péroult 1988). The IRAS 100 μm emission map of the area is shown in Figure 6. The 100 μm infrared emission towards GRB970228 is $I_{100\mu m} = 13.1$ MJy sr^{-1} . Rowan-Robinson et al. 1991 give a conversion factor between visual extinction and dust emission of $A_V/I_{100\mu m} = 0.06$ mag / MJy sr^{-1} , that was computed modeling the interstellar grains and their response to the interstellar radiation field. This relation should be valid to within approximately $\pm 30\%$. Thus we obtain a value for the extinction of $A_V = 0.79 \pm 0.21$. However, the GRB970228 field is located near the galactic anticenter and towards that direction the intensity of the radiation field declines and therefore the conversion factor is likely to be higher than the value adopted, and consequently, the extinction value underestimated.

Recently, Schlegel et al. (1998) (hereafter SFD98) have published reddening estimates based on COBE DIRBE and IRAS infrared dust emission measures. They combine DIRBE data quality calibration with IRAS resolution to get infrared measures, which they calibrate using the color of elliptical galaxies and standard extinction curves to obtain reddening estimates. They find a value for the GRB970228 direction of $A_V = 0.70 \pm 0.16$, consistent with Burstein & Heiles (1982) and the IRAS 100 μm emission with the Rowan=Robinson et al. (1991) conversion factor.

6. Discussion

We have used several methods in order to determine the galactic extinction towards the field of GRB970228. First, we have measured galaxy number counts in the HST WFPC2 images and compared them to those in the HDF, a field of known optical extinction. In order to reduce the systematic errors, we have reanalyzed the HDF using the same techniques that we utilized for the GRB field. Our object catalog for the HDF is very similar to that of the HDF team, reinforcing

the view that our selection method and magnitude determinations are appropriate. We have also checked all selected objects in the magnitude ranges studied to make sure that the different depths of the images was not influencing the number counts, as could be the case, for example, with the deblending algorithm. For instance, in the WF2 CCD image of the GRB970228 field there is a face on spiral that was over deblended. Diffraction spikes also can produce automatic selection of spurious objects. We corrected these manually. This manual rejection hardly affected our extinction estimate. Another possible source of error comes from star/galaxy separation. Again, because GRB field and the HDF have different exposures, for the same magnitude ranges, objects in the HDF are detected at a higher signal-to-noise ratio and can therefore be better classified. Moreover, the GRB field is at a much lower galactic latitude, increasing the surface number density of stars. Although the number of stars detected and rejected is low, and therefore statistics on them are poor, the number of stars detected is compatible with the expectations of the Bahcall & Soneira 1984 galactic model for this particular galactic latitude. As a worst case scenario, we also estimated the extinction with our maximum likelihood method, assuming that all objects are galaxies. In this extreme case, the value of the extinction, A_V , that we obtain is approximately 0.1 magnitudes lower than our best estimate.

Another possible concern is the effect that extinction itself and the different exposure times can have on the method. The GRB field shows considerably more extinction than the HDF and was exposed for a much shorter time. Incompleteness near the limiting magnitude of the GRB field or low surface brightness objects being assigned fainter magnitudes or being missed altogether could make us overestimate the extinction. We believe that we have taken into account these effects with the correction factor we derived from our simulations (see Section 2).

In our maximum likelihood analysis we have combined the F606W and F814W images, assuming an extinction law. If we analyze both of the images separately, we obtain consistent results when converting the extinction in the WFPC2 filter to A_V , although the errors are larger. The F814W image gives a somewhat higher estimate for A_V , as can be seen in Figure 1. The combined extinction measured, denoted by the horizontal separation between the solid and dashed lines, seems insufficient to explain the observed number counts. The combined extinction value given by the maximum likelihood method is closer to the extinction given by the F606W image than to the one given by the F814W image. The F606W observations, having approximately double the exposure time, go deeper and therefore more objects are detected in the observations taken in this filter. The F606W counts therefore have slightly more weight in the combined maximum likelihood method.

González et al. (1998) are also conducting an investigation of the galactic extinction towards this same field. One of their estimates comes from a comparison of the cumulative number counts in the GRB field and the HDF in the F606W filter. In essence, their method is very similar to our combined maximum likelihood method. It is therefore reassuring that we obtain consistent values, within the errors (Fruchter, private communication).

We have also measured the optical extinction by analyzing the spectra of three nearby stars. Star S1 is the closest object to GRB970228, only 2.9" away, and the other two are only 16.8" (S2) and 42.7" (S3) away. These stars should then give the best estimate of the extinction if it varies on small angular scales. Using stellar spectra has another advantage. A wide wavelength range is sampled and the extinction signature can, in principle, be better determined. Therefore we believe this method should provide the best estimate of the optical extinction towards GRB970228. However, the stellar spectra available are of poor signal-to-noise and do not cover blue wavelength regions that are important for determining spectral types (bluewards of H_β) and where the effects of extinction are stronger. The main contribution in our error budget is then the allowed range of spectral types. In comparison, the error due to the spectrophotometric calibration is considerably smaller. Table 1 shows the consistency between the photometric and spectrophotometric derived colors. This method, potentially superior to the others, is thus somewhat hampered by the errors involved.

The Balmer lines ratios should also provide a powerful constraint on the optical extinction. However, the two galaxy spectra taken by chance are of low signal-to-noise, as the slit happened to fall far off the galaxy centers. For galaxy G2 we are able to measure the H_α/H_β and H_γ/H_β ratios. The value obtained from the former ratio is degenerate in the internal galaxy extinction and the extinction due to our own galaxy (see Figure 4) and the error in the second ratio does not allow us to break this degeneracy. So, although we obtain a best-fit value that is consistent with our best extinction estimate, this value is unconstrained and therefore not used.

The other methods used do not measure the extinction in the optical and rely on correlations between various observed quantities and the optical extinction to get an estimate. This necessary extrapolation renders these techniques more uncertain. The correlations between hydrogen column density and color excess (or extinction), and between the infrared 100 micron emission and color excess are known to have large intrinsic scatters (e.g., Bohlin et al. 1978; Boulanger & Péroul 1988). The infrared emission has the additional disadvantage that, near the galactic plane, it depends on the galactic longitude, because the contribution of the stellar radiation field to the dust emission declines with distance from the galactic center (Rowan-Robinson et al. 1991). GRB970228 is located near the galactic anticenter at $l_{II} = 189.913^\circ$, $b_{II} = -17.941$, and it is conceivable that the relation we have used to obtain the optical extinction underestimates it. On the other hand, the value obtained by SDF98 is very similar and is based on a different calibration that does not depend on this correlation, so the effect of galactic longitude is unclear. Another concern about these methods is the spatial resolution. The resolution of the hydrogen column density maps that we have used is of the order of a degree, while the resolution of the IRAS 100 micron maps that we have used is approximately 5 arcminutes. Figure 6 shows both maps. The two maps correlate well on large angular scales. However, the resolution of the hydrogen column density map is clearly insufficient for a good determination of the extinction towards GRB970228 because there is a strong gradient in this region. The IRAS 100 micron image, with its higher resolution, demonstrates this point. Structures of a few arcminutes in size that are visible in the 100 μm map are smeared out in

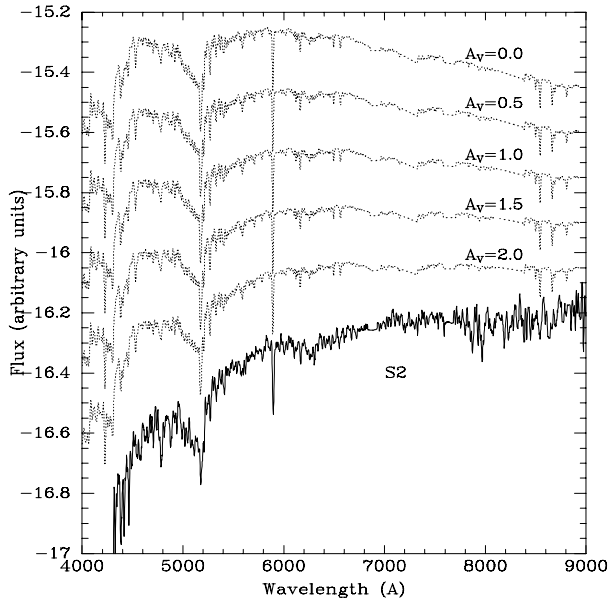


Fig. 7.— Spectrum of star S2 (solid spectrum) and a K4v star library spectrum reddened by $A_V = 0.0, 0.5, 1.0, 1.5$ and 2.0 , respectively from top to bottom (dotted spectra).

the HI image. It is important to note that the infrared emission is very knotty in the GRB region that coincides with the outskirts of a SNR centered $\sim 10^\circ$ to the East (left) outside of our image in Figure 6. It is unclear, whether material from this SNR can contribute to the extinction in the GRB field, although from the $100 \mu\text{m}$ image this seem unlikely. The IRAS 100 micron image does not provide enough resolution for a definitive conclusion.

Table 2 summarizes our measurements. We have computed the optical extinction using three different methods. We have also used correlations with neutral hydrogen and dust emission for additional estimates. The measured X-ray spectrum of the GRB afterglow provides another measurement of the extinction as well. Unfortunately, given the faintness of the GRB X-ray afterglow when observed by BeppoSAX this constraint is very weak and completely superseded by our measurements. We compute our best value for the optical extinction with the weighted average of the values obtained by the different methods. We apply two weights to average our measurements. One is inversely proportional to the relative error and the other is based on our subjective evaluation of the method reliability. We arbitrarily assign a three times larger weight to methods based on optical data than those based on other wavelengths. These weights are tabulated in Table 2 third and fourth column respectively.

It is somewhat puzzling that not all the methods used give estimates of the extinction that are consistent with each other. The two methods based on spectroscopic observations give higher values. This effect could be due to a wrong spectrophotometric calibration. However, the agreement between photometric and spectrophotometric colors (Table 1) indicates that this is not the case. A

spectral type misclassification could also yield to an overestimation of the extinction using stellar spectra. We believe that we have been very cautious assigning spectral types (see Section 3.2), which results in the large errors quoted. For example, if the value of the extinction is $A_V \sim 0.9$, star S2 had to be an M star in order to be compatible with the observed colors (or overall spectral slope). The lack of strong molecular features in the spectrum rules out this possibility. To illustrate the scope of the disagreement we plot in Figure 7 the observed spectrum of star S2 along with a stellar library spectra of a K4v star, that is reddened with an $R_V = 3.1$ extinction law of $A_V = 0.0, 0.5, 1.0, 1.5$ and 2.0 . A value of the extinction around $A_V \sim 0.9$ would imply a reddened K4v star that has a markedly different spectral slope than that of star S2. If the extinction value measured using the stellar spectra is at least $A_V \sim 1.2$ (the best value obtained with the Balmer emission line ratios agrees with such a figure), why do the other methods give a significant lower value? We believe that a plausible explanation could be variations in the extinction on angular scales < 1 arcminute. The IRAS 100 μm map provides evidence of strong variations of the dust emission on scales of a few arcminutes (Figure 6). It is therefore likely that the difference between extinction estimates derived from hydrogen and infrared dust emissions and the extinction estimate derived from the spectra of the nearby stars is due to variations on arcminute scales. However, in order to explain the difference between the extinction estimates obtained from galaxy number counts and the spectra of nearby stars, those variations would have to be on scales < 1 arcminutes. This would have to be so because the WFPC2 images cover scales of the order of one arcminutes, while stars S1 and S2, which have the most weight in the estimation using stellar spectra, are only $2.9''$ and $16.8''$ arcseconds away from GRB970228. Some support for the hypothesis of variations in the extinction on small angular scales comes from the fact that the PC1 CCD has fewer objects than expected from extrapolation of the WF CCDs counts; however, this deficit is not statistically significant.

González et al. (1998) also estimate the extinction in this field. They compare cumulative galaxy number counts and galaxy colors in the GRB970228 field to those in several other HST WFPC2 images to obtain a value of the extinction. They obtain values consistent with the SFD98 estimate.

Summarizing, our best estimate for the optimal extinction is $A_V = 1.19^{+0.10}_{-0.17}$. Such a value considerably modifies the broad-band spectral shape of the GRB970228 afterglow (Reichart et al. 1998). For example, an observed broad band $V - I_c$ color of 2.0 would deredden to an unabsorbed $V - I_c = 1.5$ and a V magnitude of 22.0 would turn into $V = 20.8$. If we were to drop the determinations of the extinction from the stellar spectra, we would obtain $A_V = 0.86 \pm 0.11$, but we feel that there is no a priori reason why these should be discarded. We emphasize that the stars lie close to and bracket the position of the GRB970228 afterglow.

7. Conclusions

We have measured the extinction towards the field of GRB970228. In making this determination, we have used the relative number counts between the WFPC2 images of the HDF and

GRB970228 fields, the spectra of three nearby stars and the Balmer line ratios of a nearby galaxy. The first method produces the tightest constraint due to the relative good statistics. The second method constitutes the best way of determining the extinction because the widest spectral range is covered and the stars lie near the direction of GRB970228. However, due to poor signal-to-noise the constraints are poor. The third method gives an unconstrained value of the extinction, although it is convenient to remark that its best value coincides with our final result within the errors. Variance among the results of these methods may indicate that the gas and dust in this direction are “mottled” or clumped on small angular scales. We have used other indirect methods based on the hydrogen column density and the dust $100\mu\text{m}$ emission. The infrared emission gives a lower estimate for the extinction than the previous methods. Combining the above techniques, weighting the optical methods more than the other indirect ones, we obtain a best value of $A_V = 1.19^{+0.10}_{-0.17}$.

The measured A_V implies that the GRB970228 afterglow is intrinsically brighter and bluer than the observed magnitudes and color. For example, in the R_c filter the intrinsic magnitudes is 1.2 brighter and the $V - I_c$ color is 0.52 magnitudes bluer than observed.

It is a pleasure to acknowledge Carlo Graziani, Daniel Reichart and Jean Quashnock, for their help, especially with regard to statistical methodology. We have also benefited from useful discussions with Mark Metzger, Cole Miller, Dave Cole and Andrew Fruchter. We thank Andrew Fruchter in particular for pointing out to us the effect on galaxy number counts of surface brightness dimming due to extinction. We thank John Tonry, Esther Hu, Len Cowie and Richard McMahon for making publicly available their spectra of the objects in the GRB97028 field. We have made extensive use of the SkyView facility developed and maintained under NASA grants at GSFC. Part of this work is based on NASA/ESA Hubble Space Telescope archival data retrieved from the archive maintained at STSci. We acknowledge support from NASA grants NAGW-4690, NAG 5-1454, and NAG 5-4406.

Table 1. Star magnitudes.

Star	V_{606}	I_{814}	$V_{606} - I_{814}$	$(V_{606} - I_{814})_{spec}$
S1	22.63 ± 0.02	21.68 ± 0.03	0.95 ± 0.04	0.93
S2	21.52 ± 0.02	20.63 ± 0.03	0.89 ± 0.04	0.93
S3	24.14 ± 0.06	22.32 ± 0.06	1.82 ± 0.09	1.88

Table 2. Extinction values.

Method	A_V	weight1	weight2
Number counts	0.89 ± 0.13	0.357	0.375
Balmer series ratios	1.27	0.000	0.000
Stars	$1.73^{+0.20}_{-0.42}$	0.291	0.375
X-ray extinction	< 2.26	0.000	0.000
$N(HI)$	0.93 ± 0.39	0.124	0.125
$I_{100\mu m}$ (correlation)	0.79 ± 0.21	0.000	0.000
$I_{100\mu m}$ (SFD98)	0.70 ± 0.16	0.228	0.125
Combined (weight1)	$1.10^{+0.10}_{-0.14}$		
Combined (weight1&2)	$1.19^{+0.10}_{-0.17}$		

REFERENCES

- Bertin, E. & Arnouts, S. 1996, *A&AS*, 117, 393
- Bahcall, J.N. & Soneira, R.M. 1984, *ApJS*, 55, 67
- Bohlin, R. C., Savage, B. D. & Drake, J. F. 1978, *ApJ*, 224, 132
- Boulangier, F. & Pérault, M. 1988, *ApJ*, 330, 964
- Brainerd, T.G. & Smail, I. 1998, *ApJ*, 494, L137
- Burstein, D. & Heiles, C. 1978, *ApJ*, 225, 40
- Burstein, D. & Heiles, C. 1982, *ApJS*, 87, 1165
- Cardelli, J. A., Clayton, G. C. & Mathis, J. S. 1987, *ApJ*, 345, 245
- Castander, F.J. & Lamb, D.Q. 1997, Proceedings of 4th Huntsville Gamma-Ray Burst Symposium, eds. C. A. Meegan, R. Preece, and T. Koshut, astro-ph/9803324
- Castander, F.J. & Lamb, D.Q. 1998, *ApJ*, submitted
- Costa, E., Feroci, M., Frontera, F., Zavattini, G., Nicastro, L., Palazzi, E., Spoliti, G., Di Ciolo, L., Coletta, A., D'Andreta, G., et al., 1997a, *IAU Circ* 6572
- Costa, E., Feroci, M., Piro, L., Cinti, M.N., Frontera, F., Zavattini, G., Nicastro, L., Palazzi, E., Dal Fiume, D., Orlandini, M., et al., 1997b, *IAU Circ* 6576
- Dickey, J. M. & Lockman, F. J. 1990, *ARA&A*, 28, 215
- Djorgovski, S.G., Kulkarni, S.R., Gal, R.R., Odewahn, S.C. & Frail, D.A. 1997, *IAU Circ* 6732
- Frontera, F., Greiner, J., Antonelli, L.A., Dal Fiume, D., Orlandini, M., Boller, T, Woges, W., et al., 1997, *IAUCirc* 6637
- Frontera, F., Costa, E., Piro, L., Muller, J.M., Amati, L., Feroci, M., Fiore, F., Pizzichini, G., Tavani, M., Castro-Tirado, A., Cusumano, G., Dal Fiume, D. et al. 1998a, *ApJ*, 493, L67
- Fruchter, A., Livio, M., Macchetto, D., Petro, L., Sahu, K., Pian, E., Frontera, F., Thorsett, S. & Tavani, M., 1997, *IAU Circ* 6747
- Galama, T., Groot, P., van Paradijs, J., Kouveliotou, C., Robinson, C.R., Fishman, G.J., Meegan, C.A., Sahu, K.C., Livio, M., Petro, L., Macchetto, F.D., Heise, J., in't Zand, J., Strom, R.G., Telting, J., Rutten, R.G.M., Pettini, M., Tanvir, N. & Bloom, J. 1997, *Nature*, 387, 479

- Galama, T., Groot, P., van Paradijs, J., Kouveliotou, C., Sahu, K.C., Livio, M., Petro, L., Macchetto, F.D. & Fruchter, A. 1998, Proceedings of 4th Huntsville Gamma-Ray Burst Symposium, eds. C. A. Meegan, R. Preece, and T. Koshut, astro-ph/9712322
- González, R.A., Fruchter, A.S. & Dirsch, B. 1998, in preparation.
- Groot, P., Galama, T., van Paradijs, J., Strom, R., Telting, J., Rutten, R.G.M., Pettini, M., Tanvir, N., et al., 1997a, IAU Circ 6584
- Groot, P., Galama, T., van Paradijs, J., Melnick, G., van der Steene, G., Bremer, M., Tanvir, N., Bloom, J., Strom, R., Telting, J., Rutten, R.G.M., et al., 1997b, IAU Circ 6588
- Heiles, C. 1975, A&AS, 20, 37
- Heiles, C. 1975, ApJ, 204, 379
- Heiles, C. & Cleary, M. N. 1979, Aust. J. Phys. Suppl., no.47
- Holtzman, J., Burrows, C.J., Casertano, S., Hester, J.J., Trauger, J.T., Watson, A.M. & Worthey, G. 1995, PASP, 107, 1065
- Horne, K. 1986, PASP, 98, 609
- Jacoby, G. H., Hunter, D. A. & Christian, C. A. 1984, ApJS, 56, 257
- Kirpatrick, J. D., Henry, T. J. & McCarthy, D. W. 1991, ApJS, 77, 417
- Klose, S., Stecklum, B. & Tuffs, R. 1997, IAU Circ 6611
- Knapp, G. R. & Kerr, F. J. 1974, A&A, 35, 361
- Margon, B., Deutch, E.W., Lamb, D.Q. & Castander, F.J. 1997, IAU Circ 6618
- Metzger, M.R., Kulkarni, S.R., Djorgovski, S.G., Gal, R., Steidel, C.C., 1997a, IAU Circ 6588
- Metzger, M.R., Cohen, J.L., Blaceslee, J.P., Kulkarni, S.R., Djorgovski, S.G., Steidel, C.C. & Frail, D.A. 1997b, IAU Circ 6631
- O'Donnell, J.E. 1994, ApJ, 422, 158
- Osterbrook, D. E., Astrophysics of Gaseous Nebulae and Active Galactic Nuclei (Mill Valley, CA: University Science Books)
- Pedichini, F., Di Paola, A., Stella, L., Buonanno, R., Boattini, A., Gandolfi, G., Costa, E., Feroci, M., Piro, L., Dal Fiume, D., Frontera, F., Nicastro, L., Palazzi, E., Heise, J., In't Zand, J. & Vietri, M., 1997, A&A, 327, L32
- Pritchett, C. & van den Bergh, S. 1977, ApJS, 34, 101

- Reichart, D.E. 1998, ApJ, 485, L57
- Reichart, D.E., Lamb, D.Q. & Castander, F.J. 1998, in preparation.
- Rowan-Robinson, M., Hughes, J., Jones, M., Leech, K., Veda, K. & Walker, D. W. 1991, MNRAS, 249, 729
- Sahu, K. C., Livio, M., Petro, L. & Macchetto, F., 1997a, IAU Circ 6606
- Sahu, K. C., Livio, M., Petro, L., Macchetto, F., van Paradijs, J., Kouveliotou, C., Fishman, G. & Meegan, C., 1997b, IAU Circ 6619
- Sahu, K. C., Livio, M., Petro, L., Macchetto, F. D., Van Paradijs, J., Kouveliotou, C., Fishman, G. J., Meegan, C. A., Groot, P. J. & Galama, T. 1997, Nature, 387, 476
- Schlegel, D.J., Finkbeiner, D.P. & Davis, M. 1998, ApJ, 500, 525 (SFD98)
- Shane, C. D. & Wirtanen, C. A. 1967, Publ. Lick Obs., 22, 1
- Silva, D.R. & Cornell, M. E. 1992, ApJS, 81, 865
- Soifer, B., Neugebauer, G., Armus, L., Metzger, M., Kulkarni, S., Djorgovski, S., Steidel, C. & Frail, D. 1997, IAU Circ 6619
- Stark, A. A., Gammie, C. F., Wilson, R. W., Bally, J. & Linke, R. A. 1992, ApJS, 79, 77
- Tonry, J. L., Hu, E. M., Cowie, L. L. & McMahan, R. G. 1997, IAUCirc 6620
- van Paradijs, J., Groot, P., Galama, T., Kouveliotou, C., Strom, R.G., Telting, J., Rutten, R.G.M., Fishman, G.J., Meegan, C.A., Pettini, M., Tanvir, N., et al 1997, Nature, 386, 686
- Vieira, E. F. & Ponz, J. D. 1995, A&AS, 111, 393
- Wijers, R.M.A.J., Rees, M.J. & Mészáros, P. 1997, MNRAS, 288, L51
- Williams, R. E., Blacker, B., Dickinson, M., Dixon, W., Ferguson, H. C., Fruchter, A. S., Giavalisco, M., Gilliland, R. L., Heyer, I., Katsanis, R., Levay, Z., Lucas, R. A., McElroy, D. B., Petro, L. & Postman, M. 1996, AJ, 112, 1335
- Yoshida, A., Kawai, N., Otani, C., Tokanai, F., Inoue, H., Murakami, T., Nagase, F., Shibata, R., et al 1997, IAUCirc 6593